Chemical Engineering Science 70 (2012) 165–175

Contents lists available at ScienceDirect

Chemical Engineering Science

journal homepage: www.elsevier.com/locate/ces

Numerical behavior of a multiscale aggregation model—coupling population balances and discrete element models

Alexander Reinhold, Heiko Briesen *

Chair for Process Systems Engineering, Technische Universität München, 85350 Freising, Germany

ARTICLE INFO

Article history:
Received 22 November 2010
Received in revised form
15 June 2011
Accepted 21 June 2011
Available online 5 July 2011

Keywords:
Aggregation
Discrete element model (DEM)
Dynamic simulation
Multiscale simulation
Nucleation
Population balance

ABSTRACT

The aggregation-rate kernel of shear-induced aggregation introduced by Smoluchowski (1917) is accurately reproduced by a discrete element model to investigate the behavior of a multiscale approach that couples discrete element simulations concurrently to a population balance model. The analyzed model comprises nucleation, growth and aggregation. From the analysis of the discrete element model an estimation for the coefficient of variation of the simulation results is derived and validated. The results of the multiscale simulations show that, in general, only a certain fraction of the total particle volume can be predicted and also that, dependent on the growth term, a biased deviation of the total volume exists. With the investigated multiscale-modeling framework the need for an analytical aggregation-rate kernel is at least in principle obsolete. Hence, the limitations of the modeling assumptions necessary to derive analytical kernels may be avoided in the future.

1. Introduction

The predictive simulation of aggregation is still not possible today. Usually, population balance equations are utilized to describe the phenomena on a macroscopic level to solve industrial-scale problems. However, the physics of aggregation is based on microscopic phenomena. Collision rates are governed by many effects: particle-mass fraction, particle shape, particle-size distribution, spatial distribution of particles and the effective flow field. Furthermore, the final aggregation rate is not identical to the collision rate and some efficiency term applies, which depends additionally on the relative motion of the colliding particles and their inter-particle forces. These variables are not even available in a population balance model. In this contribution, the term aggregation is not distinguished from coalescence and coagulation, as these mechanisms are, of course, different in nature, but are described with the same terms in a population balance and comprise similar problems to obtain a macroscale rate equation from microscale analysis.

Analytic expressions for collision rate kernels (*e.g.* the classical shear-induced or Brownian aggregation-rate kernel of Smoluchowski (1917)) require very restrictive assumptions: low particle-mass fraction, ideal spherical particles, no dependency on particle-size distribution, well-mixed compartment and a single type of mechanism. It is very unlikely that all these assumptions are truly reasonable for arbitrary cases. The Brownian aggregation-rate kernel was investigated using discrete element models by Trzeciak et al. (2004, 2006) and Heine and Pratsinis (2007), both with the result that the commonly used aggregation-rate kernel by Smoluchowski already differs significantly with a particle-mass fraction of 1%.

Mumtaz et al. (1997) obtained an analytic aggregation-rate kernel for the precipitation of calcium oxalate monohydrate by analysis of microscale mechanisms, which used mean values for the particle sizes and shear rates and constant material properties. The results were additionally validated by Hounslow et al. (2001) with excellent agreement. However, the experimental results spread around the analytic solution, which is attributed to the averaging of the particle-size distribution and shear rates in the vessel and the application of constant material properties for all experiments.

A multiscale model for granulation processes was developed by Gantt and Gatzke (2006), which used discrete element simulations to determine the coalescence kernel in advance of solving a 3-dimensional population balance model by a constant-number Monte-Carlo simulation. The model reproduced the results of the experiment, but parameters were fitted to achieve this agreement so the predictivity of this method is still open for discussion.

In our preliminary work (Reinhold and Briesen, 2009) analytic aggregation-rate kernels for shear-induced aggregation and gravitational settling were reconstructed using discrete element

* Corresponding author. Tel.: +49 8161 71 3727; fax: +49 8161 71 4510.
E-mail addresses: alexander.reinhold@tum.de (A. Reinhold), heiko.briesen@wzw.tum.de (H. Briesen).

0009-2509/$ - see front matter © 2011 Elsevier Ltd. All rights reserved.
doi:10.1016/j.ces.2011.06.041

simulations and concurrently coupled to a 1-dimensional population balance consisting of only the aggregation mechanism.

Summarizing the above studies, microscale models already exist and discrete element simulations are promising to evaluate aggregation-rate kernels with high predictivity. In principle, many assumptions can be relaxed in discrete element models: arbitrary shapes, high particle density, particle interactions or complex flow fields. Hence, predictivity need not be limited by potentially invalid assumptions.

As obtaining macroscale equations for the mechanisms on the microscale level seems to be difficult, microscale models must be coupled directly to the population balance on the macroscale level. The heterogeneous multiscale framework, for which Weinan et al. (2007) give a detailed summary, provides the required concept to analyze and derive multiscale models. In general, initializing the microscale model based on the macroscale system state is an important step. For discrete element simulations, this usually introduces random variables and, hence, the results will have a certain standard deviation. This standard deviation can be minimized by higher computational effort, but it will not vanish completely.

In contrast to Gantt and Gatzke, this study uses a 1-dimensional population balance comprising nucleation, growth and aggregation that is *concurrently* coupled to a discrete element model to calculate the required aggregation-rate kernels. One goal of this case study is to investigate the implementation of such a multiscale model. Another goal is to learn how the deviations of the aggregation-rate kernel influence the solution of the population balance equations. To achieve the latter, special effort has been made to obtain a discrete element model that perfectly reflects the analytic aggregation-rate kernel by Smoluchowski so that the analytic equation of the aggregation-rate kernel can be used to determine the difference between the multiscale model and a classical population balance model. Furthermore, an equation is derived to estimate the coefficient of variation, representing the standard deviation, based on variables available on the level of the population balance. This will be of fundamental interest, if the whole model requires a given accuracy because this reflects the uncertainty of the microscale model.

By using concurrent coupling of both multiscale levels, the complete model relates to a multiscale approach, which is called "Equation-Free" by Kevrekidis et al. (2004). This name reflects best the motivation of the studies in this contribution: eliminating the need of an analytic equation for the aggregation-rate kernel.

2. Population balance model

Population balance modeling is an established modeling technique (Ramkrishna, 2000), the model and solution technique is summarized in this section.

The particle population comprises ideal spherical particles in a well-mixed compartment. The volume v (or radius $\lambda(v)$) is the only internal coordinate. This case study comprises nucleation, growth and aggregation. The population balance equation to model this problem is given by

$$\frac{\partial \tilde{n}(v,t)}{\partial t} = -\frac{\partial G(v)\tilde{n}(v,t)}{\partial v} + \sigma_{\mathrm{nuc}}(v) + \frac{1}{2}\int_0^v r(\tilde{n},v',v-v')\,dv' - \int_0^\infty r(\tilde{n},v,v')\,dv', \tag{1}$$

where the number-based particle-size distribution is denoted by $\tilde{n}$,

$$G(v) = k_g \lambda(v)^2 \tag{2}$$

is the growth rate, which is equivalent to a constant rate of increase of the particle radius, and $\sigma_{\mathrm{nuc}}(v)$ is the source term of nucleation. In this case study, the aggregation rate is assumed to be equivalent to the collision rate of particles and no efficiency term is applied.

In the form of the population balance and the aggregation rate $r(\tilde{n},v,v')$, binary aggregation is already assumed. The aggregation-rate kernel $\beta(v,v')$ is, hence, usually separated with:

$$r(\tilde{n},v,v') = \beta(v,v')\tilde{n}(v)\tilde{n}(v'). \tag{3}$$

As well as process parameters like shear rate, the aggregation-rate kernel may, in general, depend on the particle-mass fraction or particle-size distribution (Trzeciak et al., 2006; Heine and Pratsinis, 2007), which is in contrast with commonly used aggregation-rate kernels.

The analytically derived aggregation-rate kernels require the assumption of spherical and homogeneously distributed particles, as well as binary aggregation (Ramkrishna, 2000). Hence, the assumptions for the population balance in Eq. (1) are mandatory, if analytical aggregation-rate kernels are used. In this contribution only shear-induced aggregation is considered. The aggregation-rate kernel is given by:

$$\tilde{\beta}(v,v') = \frac{4}{3}\gamma(\lambda(v)+\lambda(v'))^3, \tag{4}$$

where γ is the shear rate (Smoluchowski, 1917).

The internal coordinate of the population balance is discretized by a moving pivot technique (Kumar and Ramkrishna, 1997). With the applied discretization scheme, the particle-size distribution is represented by particle densities n_i for a total number of n_{int} intervals with corresponding particle volumes v_i. Hence, the particle-size distribution is given by: $\tilde{n}(v) = \sum_{i=1}^{n_{\mathrm{int}}} \delta(v_i - v)n_i$, where $\delta(.)$ is the Dirac impulse.

The resulting system of ordinary differential equations is integrated by a forward Euler scheme to ensure a simple algorithm for analysis. A small enough step size has been chosen to prevent any instabilities.

3. Multiscale framework

Weinan et al. (2007) give a detailed overview of the heterogeneous multiscale framework. The term heterogeneous emphasizes that multiple scales may be of very different nature and, hence, comprise very different modeling techniques.

The common task is to solve a problem on a macroscale level, but the equations on this level are either not completely available or not valid. On the other hand, a model on a microscale level is available, but the evaluation is too computationally expensive to solve the problem on this scale. Heterogeneous multiscale modeling provides a framework to analyze the problem and derive a multiscale model, which solves the problem based on equations on the macroscale *and* microscale level with a computational effort much less than solving the problem completely on the microscale level. Furthermore, it is distinguished between serial coupling, where the microscale simulations are evaluated in advance, and concurrent coupling, where microscale simulations are evaluated simultaneously when solving the macroscale model.

The heterogeneous multiscale framework gives a data-driven approach to design an appropriate multiscale model. The system state is introduced on macroscale, U, and on microscale, u. Some parameters (D for macroscale and d for microscale) exist on both layers with abstract constitutive relations for the macroscale $F(U,D)=0$ and microscale $f(u,d)=0$, where the interesting point for a macroscale model is not the equation F, but the variable D, which is required. As state variables and parameters

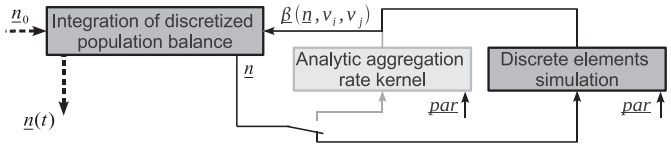

Fig. 1. Scheme of multiscale framework.

are introduced on both levels, their connection is denoted by some abstract operators. To obtain U from u, the system state is *compressed*. To obtain u from U, the system state must be *reconstructed*. To obtain D from the underlying microscale model, *data estimation* is required. And finally, the constitutive equations on the macroscale level may give *constraints* on the microscale level *via* $f(u,d)$.

3.1. Case study

In this study, the aggregation-rate kernel is assumed to be the missing equation of the macroscale population balance model ($F(U,D)=0$). It will be estimated using a discrete element model on the microscale level. From previous studies (Mumtaz et al., 1997; Hounslow et al., 2001) it is known that the aggregation-rate kernel depends on the mean values of the particle size, shear rate and supersaturation or growth rate, where it is argued that the distributions of these parameters affect the spread of experimental results compared to modeling results. Hence, it is furthermore assumed that the aggregation-rate kernel depends on many parameters in such a way that serial coupling is not reasonable and concurrent coupling must be applied.

The resulting multiscale approach is already characterized by Kevrekidis et al. (2004) as "Equation-free". Fig. 1 illustrates the framework. By integration of the discretized population balance model, aggregation-rate kernels are required each time step. Instead of using the analytic aggregation-rate kernel (the equation $F(U,D)=0$ on the macroscale), the current particle-size distribution $\underline{n}=(n_1,\ldots,n_{n_{\text{int}}})^T$ is taken (the macroscale state U) to generate a discrete population of particles (reconstruction of the microscale state u) to evaluate the discrete element simulation on the microscale level and finally estimate the required aggregation-rate kernels (data estimation for D).

The reconstruction operator is part of the initialization step of the discrete element simulation, which is described in Section 4.1, and the data estimation operator will be represented in Section 4.5.

It should be noted that this case study does not aim to solve a real problem on the macroscale level, nor does it currently save computational effort. This research tries more to address fundamental problems of multiscale modeling for population balances, which is in its infancy: what happens to the population balance model, if an underlying microscale model is used to predict aggregation-rate kernels and how to achieve such a model?

4. Discrete element model

Discrete element models originated from the analysis of granular matter (Cundall and Strack, 1979; Pöschel and Schwager, 2005), but they have also been already used to examine aggregation mechanisms (Gantt and Gatzke, 2006; Trzeciak et al., 2006; Heine and Pratsinis, 2007).

To provide a proof of principle, the assumptions for the analytical aggregation-rate kernel for shear-induced aggregation are reconstructed in the discrete element model. The results for the discrete element model will show that no systematic error is present, which must be emphasized to be of major importance because all deviations observed later on in the multiscale model stem from the nature of the multiscale model and not from an incorrect microscale model. Additionally, the presented microscale model provides an example to understand the details that need to be considered if a general aggregation-rate kernel is calculated using discrete element simulations.

The basic modeling assumptions are given in the literature and are as follows: spherical particles, dilute system, binary collisions, homogeneously distributed particles and stochastically independent collisions. The latter assumption means that the collision probability of two particles is not influenced by collisions of other particles. None of these assumptions are necessary for a discrete element simulation. However, with the given population balance, the assumption of binary collisions is mandatory. To overcome this assumption, the source and sink terms of aggregation in the population balance could be evaluated directly, without the introduction of an aggregation rate or aggregation-rate kernel. With a discrete element simulation a small part of the particle population is simulated and the birth and death rate of particles are available as the very first result. Scaling these results to the total number of particles in the population is easy to apply and the introduction of an aggregation rate or aggregation-rate kernel is superfluous. This is one example, where modeling assumptions (in this case binary collisions) are not required at all. However, for this case study the aggregation-rate kernel is still used as the simulation result because it can directly be compared to the analytic aggregation-rate kernel.

The discrete element simulation consists of three general parts. First, a set of particles is initialized, then a given time span is evaluated and finally the gathered information is evaluated at the end of each simulation.

4.1. Initialization

Using particle volume as the size coordinate for population balances is useful because of mass conservation, while the particle radius is more appropriate for the discrete element simulation. Collisions are easily evaluated by particle radii. For the discrete element simulation n_{sim} particles p_k are sampled, each with particle radius $\lambda(p_k)$ and position $\vec{s}(p_k)$.

With the assumption of homogeneously distributed particles, the position of each particle is sampled by a uniform distribution in the simulation volume:

$$V_{\text{sim}}=\frac{N}{\sum_i n_i}. \tag{5}$$

This may lead to the artifact of overlapping particles. Other initial placement algorithms that directly avoid overlapping of particles are available but would immediately violate the assumptions made for the derivation of the analytical kernel. They would result in the particle positions no longer being independent from each other. This would consequently imply that the collisions are also no longer stochastically independent from each other. In a more complex system the initial particle placement would have to be reconsidered.

The simulation volume is a rectangular box, not necessarily cubic. It has the dimensions x_{width}, y_{width} and z_{width}, where the particles move parallel to the x-axis and particle velocities increase with the vertical y-axis. A sketch is shown in Fig. 2.

The particle size is sampled randomly from the particle-size distribution with the probability distribution:

$$P_i=P(\lambda(p_k)=\lambda(v_i))=\frac{n_i}{\sum n_i}. \tag{6}$$

With N_i being the number of particles with volume v_i, the expectation of N_i is $\mu_{N_i}=n_i V_{\text{sim}}$. The reconstruction of n_i by N_i is

given by $n_i = N_i/V_{\text{sim}}$. It is important to note that the particle-size distribution is generally not reconstructed perfectly in a single simulation. However, the expectation of the reconstructed particle-size distribution μ_{n_i} is correct. There may not exist a particle for each particle volume v_i. The values $\lambda_{\min}$ and $\lambda_{\max}$ denote the minimum and maximum existent particle radii in an initialized discrete element simulation.

4.2. Simulation steps

The velocity of each particle is given by it's position and shear rate γ. No inter-particle forces apply. During the simulation, the equation of motion,

$$\frac{\partial \vec{s}(p_k)}{\partial t} = \begin{pmatrix} 0 & \gamma & 0 \\ 0 & 0 & 0 \\ 0 & 0 & 0 \end{pmatrix} \vec{s}(p_k), \tag{7}$$

is integrated, using a forward Euler scheme. At each time step, all particle pairs are checked for collisions and, with the assumption of binary collisions, are counted in the variables $C_{(i,j)}$, where the indices i and j refer to particle sizes v_i and v_j. It is not possible to ensure that all collisions are detected.

For a given time step the particles may not overlap before and after the step while a collision have taken place during the step. This systematic error can be limited by choosing time steps small enough to preserve a certain degree of accuracy. For a proper choice of Δt consider that two particles in a pure shear flow can only aggregate if the distance between the streamlines they are following is smaller than the sum of their radii. In the direction of the streams the maximum displacement of the two particles which need to be considered for collision detection is $(\lambda(p_k)+\lambda(p_l))\gamma\Delta t$ which represents the worst case. If the streamlines the particles follow have a distance from each other larger than $\lambda(p_k)+\lambda(p_l)$ they will never collide. If the stream lines are closer, the relative displacement in the given time step will be smaller so that larger time steps are less of an issue. Based on the worst-case scenario we restrict the maximum displacement to be a fraction k_λ of $(\lambda(p_k)+\lambda(p_l))$, which results in the following constraint for the time step length:

$$\Delta t \leq \frac{k_\lambda}{\gamma}. \tag{8}$$

The choice of the value of is based on simulation studies and is discussed in Section 6.4.

The link-cell algorithm (Pöschel and Schwager, 2005) is used to reduce computational complexity. As the link-cell algorithm does not alter simulation results, details are not discussed here. Furthermore, periodic boundary condition applies, as shown in Fig. 2.

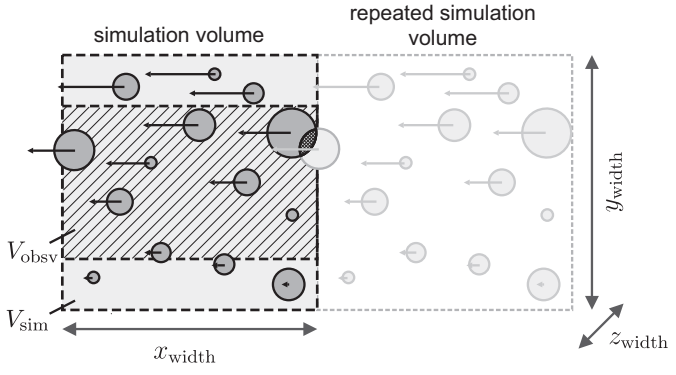

Fig. 2. Set-up of a discrete element simulation.

4.3. Estimation of aggregation-rate kernel

The aggregation-rate kernel reflects the probability of a particle pair aggregating in unit time. Adapting Eq. (3) to variables of the discrete element simulation yields

$$\frac{C_{(i,j)}}{T_{\text{sim}} V_{\text{sim}}} = \beta_{(i,j)} \frac{N_i N_j}{V_{\text{sim}}^2} \Longleftrightarrow \beta_{(i,j)} = C_{(i,j)} \frac{V_{\text{sim}}}{T_{\text{sim}} N_i N_j}, \tag{9}$$

from which the aggregation-rate kernel $\beta(v_i,v_j) \approx \beta_{(i,j)}$ can be calculated. With this step, the *framework* of the discrete element simulation is described. However, Eq. (9) is far away from being accurate because it does not reflect the discrete nature of the simulation. Furthermore, the handling of collisions and the question "what happens, if a collision is detected?" are non-trivial.

4.4. Collision detection and handling

If a collision is detected, it is counted in variables $C_{(i,j)}$ for particle pairs of sizes v_i and v_j. Keeping both particles in the system with no alteration would likely result in the collision condition being fulfilled again in the next time step, like shown in Fig. 3, and the same collision would be counted twice or more. Hence, some behavior must be introduced for collision handling. Based on this collision handling, some details for an accurate estimation of the aggregation-rate kernel will be discussed additionally in this section.

Executing the aggregation by substituting the particle pair by a particle of larger size has been done in the simulations of Heine and Pratsinis (2007). However, this alters the particle-size distribution, which is not favorable, as the simulation is expected to calculate the aggregation rate for the current system state and particle-size distribution. To achieve this, the total simulation time must be limited to relatively small times, to conserve the current particle-size distribution. This is unfavorable because the computational effort to initialize the system scales quadratic with the total particle number and cannot be neglected.

Removing both particles has been done in simulations by Trzeciak et al. (2004, 2006). If these particles are not replaced, this will again alter the particle-size distribution. Reinitializing these two particles is very complicated and may lead to stochastically dependent collisions, which was found by Trzeciak et al. (2006) for Brownian coagulation.

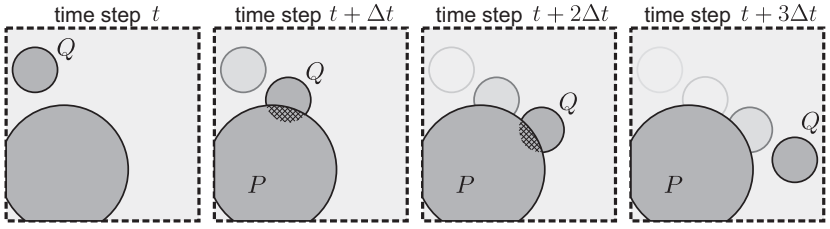

Fig. 3. Invalid double-counting of collisions.

A new approach is proposed to resolve this conflict. It is derived from the assumption of stochastically independent collisions, which will not hold in realistic situations, but reflects the modeling assumptions of the analytic aggregation-rate kernel. For each particle there exists a list of ignored particles. If a collision is detected, the other collision partner is added to this list. A collision is then only detected if the collision condition is fulfilled *and* the opposing collision partner is not in the list of ignored particles. No collision is counted twice in subsequent time steps and the total particle-size distribution is not altered. One particle can collide with several particles during one simulation, which fulfills the modeling assumption of stochastically independent collisions.

However, it must be ruled out that any pair of collision partners meet again due to periodic boundary conditions (Fig. 4). This second collision would not be detected because of the ignored-particle list. In addition, this collision would be stochastically dependent on the first one, which does not contradict the modeling assumptions, but stochastically dependent collisions do not enhance accuracy of the simulation results. The maximum relative velocity between two particles that could collide is $2\lambda_{\max}\gamma$. To exclude these cases, this relative velocity must not span the width x_{width} of the system during a whole simulation, which limits the total simulation time to:

$$T_{\text{sim}} < \frac{x_{\text{width}}}{2\lambda_{\max}\gamma}. \tag{10}$$

Using periodic boundary conditions implies that collisions are counted between particles on the bottom and on the top of the box. Obviously, this is invalid, because of the relative velocities of the corresponding particles. Hence, collisions of this type are ruled out. It follows subsequently that a particle on the bottom of the box cannot have a collision partner underneath it. This conflicts with the assumption of homogeneously distributed particles. Each particle is supposed to have an identical environment. To overcome this issue, collisions are only counted if the y-coordinate of the contact point of the collision, defined by $y_{\text{collision}} = (\lambda(p_k)y(p_l)+\lambda(p_l)y(p_k))/(\lambda(p_k)+\lambda(p_l))$, fulfills $2\lambda_{\max} < y_{\text{collision}} < y_{\text{width}}-2\lambda_{\max}$. All particles of these collisions observe an equal environment concerning the region of interest for collisions. The volume where collisions are counted differs from the simulation volume and is given by:

$$V_{\text{obsv}} = V_{\text{sim}}-4\lambda_{\max}x_{\text{width}}z_{\text{width}}. \tag{11}$$

With regard to the initialization of particle positions, there is some probability $P_{\text{init},(i,j)}$ that two distinct particles of sizes v_i and v_j fulfill the collision condition just after initialization. This probability has nothing to do with the aggregation mechanism. Collisions of this types are checked and the opposing particles are written to the respective lists of ignored particles without counting these collisions. This results in a slightly lower particle density $(1-P_{\text{init},(i,j)})N_i/V_{\text{sim}}$ being observed by particles of size v_j. This could be resolved by randomly introducing additional particles of size v_i only for particles of size v_j with an expectation of $P_{\text{init},(i,j)}n_iV_{\text{sim}}$ additional particles. As the amount of particles to add is typically $P_{\text{init},(i,j)}n_iV_{\text{sim}} \ll 1$, this error can be neglected compared to the standard deviation of the simulation result. No additional particles are added to the system, but the deviation of the particle-size distribution will be accounted for in calculating the aggregation-rate kernel. This is done with the assumption that the aggregation-rate kernel is not highly sensitive to the particle-size distribution. In fact the aggregation-rate kernel for shear-induced aggregation is totally independent from the distribution.

4.5. Modified estimation of aggregation-rate kernel

As all details of the simulation are fixed, the naïve equation (9) can be redefined to reflect the nature of the discrete element simulation. The aggregation-rate kernel reflects the probability of a particle pair aggregating in unit time. $C_{(i,j)}/T_{\text{sim}}$ collisions are counted per unit time in the observation volume. The total number of collision partners in the simulation volume is N_iN_j for $i\neq j$ and $N_i(N_j-1)/2$ for $i=j$, which must be reduced by the factor $(1-P_{\text{init},(i,j)})$ as a result of the initialization of the system. This results in $(1-P_{\text{init},(i,j)})N_i(N_j-\delta_{i,j})/((1+\delta_{i,j})V_{\text{sim}})$ collision partners per unit volume, which must be scaled by the factor $V_{\text{obsv}}/V_{\text{sim}}$ to the volume where collisions are observed. This yields the statistically evaluated aggregation-rate kernel:

$$\hat{\beta}_{(i,j)} = \hat{C}_{(i,j)}\frac{V_{\text{sim}}^2}{T_{\text{sim}}V_{\text{obsv}}}\frac{1+\delta_{i,j}}{(1-P_{\text{init},(i,j)})N_i(N_j-\delta_{i,j})}. \tag{12}$$

5. Stochastic analysis of simulation results

As both the size and position of particles are randomized during initialization, the simulation results are random as well. In this section, the coefficient of variation of the aggregation-rate kernel will be derived by approximations and some standard textbook probability theory (Beyer et al., 1995). The result will be further approximated to variables available on the multiscale level of the population balance, which makes it particularly useful if the accuracy on this level must be determined.

The starting point is Eq. (12), which consists of three random variables: the number of counted collisions $C_{(i,j)}$ and the number of particles N_i and N_j. Obviously, for $i=j$ just two random variables are present. The cases $i=j$ and $i\neq j$ are handled without distinction.

The probability of a single particle being of size v_i is given by $P_i = n_i/\sum_j n_j$. The random variable N_i is binomially distributed with mean $\mu_{N_i} = NP_i$ and standard deviation $\sigma_{N_i} = \sqrt{NP_i(1-P_i)}$. The number of particle pairs, which *may be counted* by $C_{(i,j)}$ is a function of the random variables N_i and N_j and is defined by:

$$N'_{i,j} = \frac{N_i(N_j-\delta_{i,j})}{1+\delta_{i,j}}. \tag{13}$$

Given a particle pair of sizes v_i and v_j, the probability that a collision is observed and counted by $C_{(i,j)}$ is denoted by $P_{\text{coll},(i,j)}$. This probability includes the case that the particle pair cannot be counted by $C_{(i,j)}$ because it fulfills the collision condition just after initialization. The probability distribution of counted collisions,

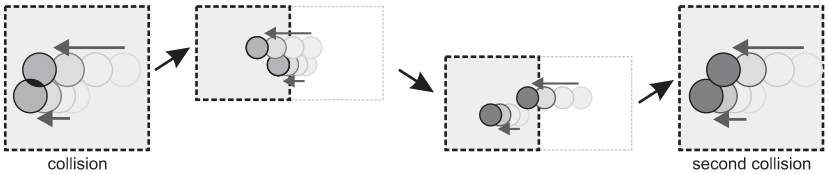

Fig. 4. Double-counting of collisions due to periodic boundary conditions.

with the condition of $N'_{(i,j)}$ particle pairs being present, is binomially distributed:

$$P(C_{(i,j)}|N'_{(i,j)}) = \binom{N'_{(i,j)}}{C_{(i,j)}} (P_{\mathrm{coll},(i,j)})^{C_{(i,j)}} (1-P_{\mathrm{coll},(i,j)})^{N'_{i,j}-C_{(i,j)}}, \tag{14}$$

with mean $\mu_{C_{(i,j)}} = N'_{(i,j)} P_{\mathrm{coll},(i,j)}$ and standard deviation $\sigma_{C_{(i,j)}} = \sqrt{N'_{(i,j)} P_{\mathrm{coll},(i,j)}(1-P_{\mathrm{coll},(i,j)})}$.

In the next step, the binomial distributions are approximated by normal distributions, which gives reasonable results for $\mu_{C_{(i,j)}} \geq 4$. Because of $P_{\mathrm{coll},(i,j)} \ll 1$ it follows that $\mu_{N_i} \gg 1$ and $\mu_{N_j} \gg 1$, from which it follows that approximating the distribution of $C_{(i,j)}$ being normally distributed implies that approximating N_i and N_j being normally distributed is reasonable as well. Furthermore, from probability theory it holds that given a normal distribution, each linear transformation of it is normally distributed as well.

The random deviations of $N'_{(i,j)}$ are of minor importance. Any N_k can be expressed with a linear transformation of the standard normal distributions X_k ($\mu_{X_k} = 0$, $\sigma_{X_k} = 1$):

$$N_k = \mu_{N_k} + \sigma_{N_k} X_k. \tag{15}$$

$N'_{(i,j)}$ is then transformed to:

$$N'_{(i,j)} = \frac{(\mu_{N_i} + \sigma_{N_i} X_i)(\mu_{N_j} + \sigma_{N_j} X_j - \delta_{i,j})}{1+\delta_{i,j}} \tag{16}$$

$$= \frac{(\mu_{N_j} - \delta_{i,j})\mu_{N_i} + \mu_{N_i}\sigma_{N_j} X_j + (\mu_{N_j} - \delta_{i,j})\sigma_{N_i} X_i + \sigma_{N_i}\sigma_{N_j} X_i X_j}{1+\delta_{i,j}}. \tag{17}$$

As μ_{N_i} and μ_{N_j} are large, all terms apart from the product $\mu_{N_i}\mu_{N_j}$ are relatively small. Hence, the terms containing the randomly distributed variables X_i and X_j can be neglected, even though experience shows that these random deviations of $N'_{(i,j)}$ improve the approximation of $\hat{\beta}_{(i,j)}$ being normally distributed. They smooth out the steps of the binomially distributed number of counted collisions $C_{(i,j)}$. Hence, $N'_{(i,j)}$ is assumed not to be random in the following part of this section.

By approximating the binomial distribution of $C_{(i,j)}$ by a normal distribution, using the approximation of $N'_{(i,j)}$ being constant and applying the linear transformation (Eq. (12)) it follows that the statistically evaluated aggregation-rate kernel $\hat{\beta}_{(i,j)}$ is normally distributed with mean:

$$\mu_{\hat{\beta}_{(i,j)}} = \mu_{C_{i,j}} \frac{V_{\mathrm{sim}}^2}{T_{\mathrm{sim}} V_{\mathrm{obsv}}} \frac{1+\delta_{i,j}}{(1-P_{\mathrm{init},(i,j)}) N_i (N_j - \delta_{i,j})}, \tag{18}$$

and standard deviation:

$$\sigma_{\hat{\beta}_{(i,j)}} = \sigma_{C_{(i,j)}} \frac{V_{\mathrm{sim}}^2}{T_{\mathrm{sim}} V_{\mathrm{obsv}}} \frac{1+\delta_{i,j}}{(1-P_{\mathrm{init},(i,j)}) N_i (N_j - \delta_{i,j})}, \tag{19}$$

which can be expressed as:

$$\sigma_{\hat{\beta}_{(i,j)}} = \sqrt{\mu_{\hat{\beta}_{(i,j)}}} \sqrt{\frac{V_{\mathrm{sim}}^2}{T_{\mathrm{sim}} V_{\mathrm{obsv}}} \frac{1+\delta_{i,j}}{(1-P_{\mathrm{init},(i,j)}) N_i (N_j - \delta_{i,j})}}. \tag{20}$$

using Eq. (18) and approximating $(1-P_{\mathrm{coll},(i,j)}) \approx 1$ because $P_{\mathrm{coll},(i,j)} \ll 1$.

The derived standard deviation refers to the absolute error, which makes it difficult to rate the accuracy of the discrete element model without a fixed aggregation-rate kernel. The coefficient of variation refers to the relative error and therefore is more appropriate to rate the accuracy of estimated aggregation-rate kernels. The coefficient of variation is defined by:

$$\theta_{\hat{\beta}_{(i,j)}} = \frac{\sigma_{\hat{\beta}_{(i,j)}}}{\mu_{\hat{\beta}_{(i,j)}}} = \frac{1}{\sqrt{\mu_{\hat{\beta}_{(i,j)}}}} \sqrt{\frac{V_{\mathrm{sim}}^2}{T_{\mathrm{sim}} V_{\mathrm{obsv}}} \frac{1+\delta_{i,j}}{N_i (N_j - \delta_{i,j})} \frac{1}{1-P_{\mathrm{init},(i,j)}}}. \tag{21}$$

The variables in this equation can be approximated with $V_{\mathrm{obsv}} \approx V_{\mathrm{sim}} = N/\sum_k n_k$, $P_{\mathrm{init},(i,j)} \approx 0$ and $N_i(N_j - \delta_{i,j})/V_{\mathrm{sim}}^2 \approx n_i n_j$, which finally yields:

$$\tilde{\theta}_{\hat{\beta}_{(i,j)}} = \frac{1}{\sqrt{\mu_{\hat{\beta}_{(i,j)}}}} \sqrt{\frac{1+\delta_{i,j}}{T_{\mathrm{sim}} N} \frac{\sum_k n_k}{n_i n_j}}. \tag{22}$$

With the term $1/\sqrt{\mu_{\hat{\beta}_{(i,j)}}}$, large aggregation-rate kernels are estimated with higher accuracy. Furthermore, the term $\sum_k n_k/(n_i n_j)$ implies that the aggregation-rate kernel in denser systems is estimated with a higher accuracy. Both observations are connected to the fact that more collisions are counted in dense systems or with a higher aggregation-rate kernel, which reduces the coefficient of variation of $C_{(i,j)}$, from which the probability distribution of $\hat{\beta}_{(i,j)}$ is derived from. The effect on the simulation accuracy is the same for scaling the total simulation time T_{sim} or the total number of particles N. As increasing N significantly increases the time for initializing the system, increasing the simulation time T_{sim} is preferable. Aggregation-rate kernels of the same size fraction $i=j$ have a coefficient of variation, which is larger by the factor of $\sqrt{2}$, compared to $i \neq j$.

From Eq. (21) it follows that the volume, V_{obsv}, where collisions are observed should be maximized. Maximizing V_{obsv} means maximizing y_{width} because of Eq. (11). In contrast, as the simulation time is limited by x_{width} in Eq. (10), x_{width} should be maximized. For simulations presented here, the limits $x_{\mathrm{width}} \geq 6\lambda_{\max}$ and $y_{\mathrm{width}} \leq 200\lambda_{\max}$ apply, where y_{width} is maximized.

Eq. (22) is of fundamental interest if the accuracy of the overlying population balance model is to be controlled. If a guess for the aggregation-rate kernel β is available, the simulation parameters can be chosen in such a way as to guarantee a certain level of accuracy. Furthermore, an estimation for the aggregation-rate kernel β is available after a simulation run and, hence, the accuracy can be estimated properly *a posteriori*.

6. Results of the discrete element model

The results of evaluating a high number of discrete element simulations are used to validate that the expectation value $\mu_{\hat{\beta}_{(i,j)}}$ (Eq. (18)) of $\hat{\beta}$ (Eq. (12)) equals the analytic aggregation-rate kernel $\tilde{\beta}_{(i,j)}$ in Eq. (4). This will prove that all modeling assumptions are properly implemented in the discrete element model. The estimate of the coefficient of variation in Eq. (22) will be validated to approximately reflect the real coefficient of variation. In the subsequent section, the results of evaluating a broad spectrum of particle sizes by single simulations are presented to ensure validity. The parameter k_λ is fixed for the multiscale coupling in the final subsection by analyzing the relative error in dependence of k_λ. But beforehand, some statistics and definitions are required to carry out these validations (Beyer et al., 1995).

6.1. Statistic definitions for validation

For the following statistic analysis, a level of significance $\alpha = 1\%$ applies. The empirical mean is denoted by $\hat{\mu}_{\beta_{(i,j)}}$, the empirical standard deviation is denoted by $\hat{\sigma}_{\hat{\beta}_{(i,j)}}$ and the empirical coefficient of variation is defined by $\hat{\theta}_{\hat{\beta}_{(i,j)}} = \hat{\sigma}_{\hat{\beta}_{(i,j)}}/\mu_{\hat{\beta}_{(i,j)}}$. The relative error is defined by $\delta_{\hat{\beta}_{i,j}} = (\tilde{\beta}_{i,j} - \hat{\beta}_{i,j})/\tilde{\beta}_{i,j}$ for a single simulation or by $\delta_{\hat{\mu}(\hat{\beta}_{(i,j)})} = (\tilde{\beta}_{i,j} - \hat{\mu}_{\hat{\beta}_{(i,j)}})/\tilde{\beta}_{i,j}$ for estimates from multiple simulations. To determine confidence limits to the point estimates $\mu_{\beta_{(i,j)}} = \hat{\mu}_{\beta_{(i,j)}}$ and $\theta_{\beta_{(i,j)}} = \hat{\theta}_{\beta_{(i,j)}}$, an assumption for the probability

distribution $\hat{\beta}_{(i,j)}$ is required. We retain the assumption of $\hat{\beta}_{(i,j)}$ being normally distributed.

6.2. Simulation results for large numbers of simulations

For a first detailed analysis, the discrete element model was run $n_{\mathrm{sim}} = 10^6$ times with the following parameters: $\gamma = 5\ \mathrm{m\ s^{-1}}$, $v_1 = 4\ \mu\mathrm{m}$, $v_2 = 8\ \mu\mathrm{m}$, $n_1 = n_2 = 10^{13}\ \mathrm{m^{-3}}$, $N = 6000$, $T_{\mathrm{sim}} = 0.5\ \mathrm{s}$ and $k_\lambda = 1/30$. The particle-mass fraction was $\varphi = 2.41\%$. The calculated aggregation-rate kernels $\hat{\mu}_{\hat{\beta}_{(1,1)}}$, $\hat{\mu}_{\hat{\beta}_{(2,2)}}$ and $\hat{\mu}_{\hat{\beta}_{(1,2)}}$ have relative errors at -0.0119%, 0.0029% and 0.0007%, respectively. The corresponding confidence limits imply limits of the relative errors of $\pm 0.0514\%$, $\pm 0.0182\%$ and $\pm 0.0198\%$. The different confidence levels are connected to the different values of the aggregation-rate kernels with reference to Eq. (22). No significant error and therefore no systematic error can be observed with an accuracy up to 0.0182%.

Fig. 5 shows the relative cumulated frequency distributions of the aggregation-rate kernels. They have very good agreement with the corresponding normal distributions. However, small steps can be observed for the results of $\hat{\beta}_{(1,2)}$. These steps correspond to the binomial distribution of the counted collisions $C_{(1,2)}$, which are not smoothed out by the randomly distributed number of possible collision partners $N'_{(1,2)}$ (Eqs. (13) and (14)). The reason for this observation is that N_2 is a function of N_1 with: $N_2 = N - N_1$, from which follows that X_2 is dependent on X_1 by Eq. (15). Evaluating this case for Eq. (17) yields

$$N'_{(1,2)} = (\mu_{N_1}\mu_{N_2} + (\mu_{N_2}\sigma_{N_1} - \mu_{N_1}\sigma_{N_2})X_1 + \sigma^2_{N_1}X_1^2). \tag{23}$$

For $n_1 = n_2$, this eliminates the normally distributed term X_1 completely, which leaves the term X_1^2, which is Chi-square distributed with one degree of freedom. For the cases $i=j$ Eq. (17) yields:

$$N'_{(i,i)} = \tfrac{1}{2}(\mu^2_{N_i} - \mu_{N_i} + (2\mu_{N_i} - 1)\sigma_{N_i}X_i + \sigma^2_{N_i}X_i^2), \tag{24}$$

where the normally distributed term X_i is present and more significant than the Chi-square distributed term X_i^2. This shows that the probability distribution of $N'_{(i,j)}$, which was neglected by the derivations in Section 5, improves the assumption that $\hat{\beta}_{(i,j)}$ is normally distributed by smoothing out the steps of the binomially distributed variable $C_{(i,j)}$. It is also apparent that the terms X_i, X_j and X_iX_j are of only minor significance, as was assumed.

Fig. 5 also shows that the estimated coefficient of variation by Eq. (22) is slightly smaller than the statistically evaluated coefficient of variation. In numbers, for $\hat{\beta}_{(1,1)}$ it is $\tilde{\theta}_{\hat{\beta}_{(1,1)}} = 19.76\%$, where it should be in the confidence limits of $19.90\% < \theta_{\hat{\beta}_{(1,1)}} < 20.05\%$. For $\hat{\beta}_{(2,2)}$ it is $\tilde{\theta}_{\hat{\beta}_{(2,2)}} = 6.99\%$, where it should be in the confidence limits of $7.05\% < \theta_{\hat{\beta}_{(2,2)}} < 7.10\%$. And for $\hat{\beta}_{(1,2)}$ it is $\tilde{\theta}_{\hat{\beta}_{(1,2)}} = 7.61\%$, where it should be in the confidence limits of $7.65\% < \theta_{\hat{\beta}_{(1,2)}} < 7.71\%$. The estimation of the coefficient of variation by

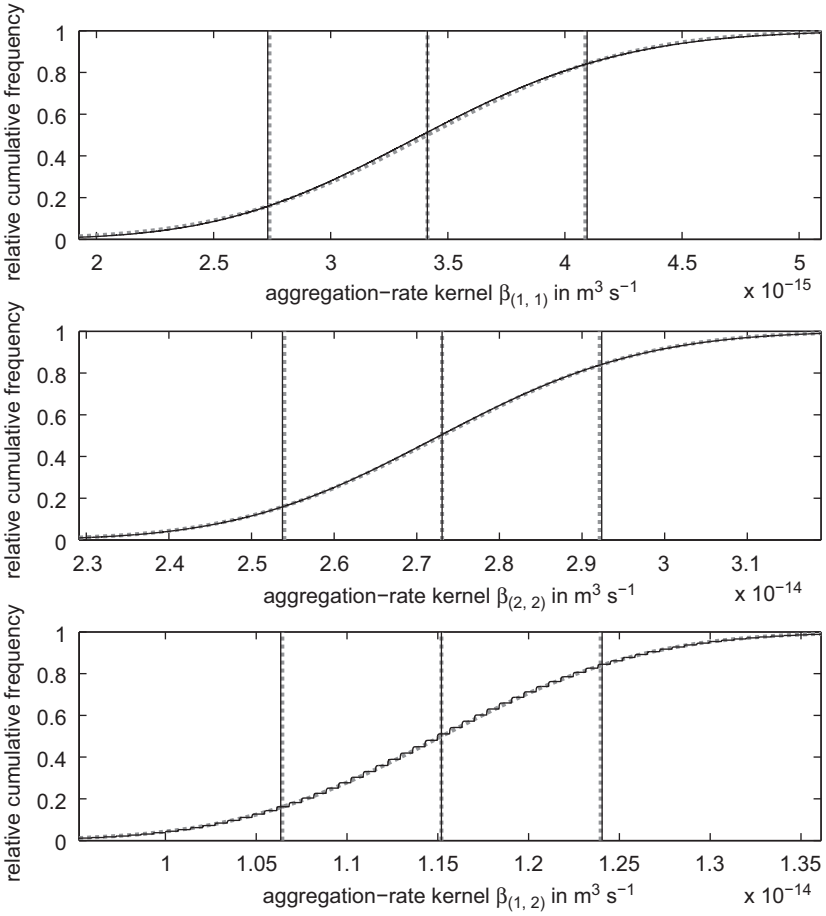

Fig. 5. Relative cumulative frequency distribution of aggregation-rate kernels $\beta_{(1,1)}$, $\beta_{(2,2)}$ and $\beta_{(1,2)}$. Thin black lines are the direct empirical data: relative cumulative frequency distribution, empirical mean (vertical line in the middle), standard deviation (additional vertical lines, that value away from the empirical mean). Bold dashed gray lines are cumulative probability distribution of a normal distribution with mean and standard deviation corresponding to empirical data, analytic aggregation-rate kernel in the middle, estimation of the standard deviation (from Eq. (22)) drawn that distance away from the empirical mean.

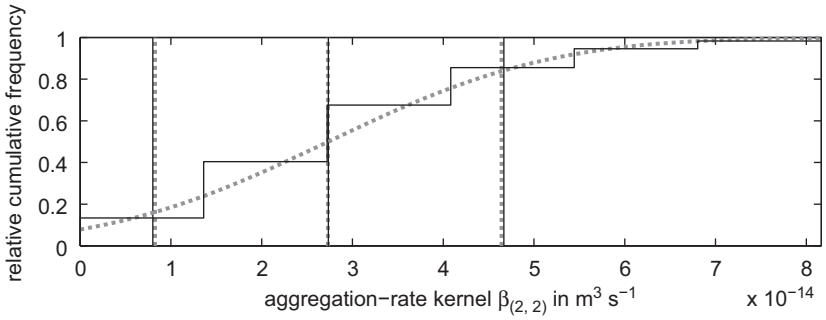

Fig. 6. Relative cumulative frequency distribution of an aggregation-rate kernels with $\mu_{C_{(2,2)}} \approx 2$. Description of graph as in Fig. 5.

Eq. (22) underestimates the real coefficient of variation, but still yields an excellent approximation.

Fig. 6 shows the relative cumulated frequency distribution of the aggregation-rate kernels from simulations with the mean number of counted collisions: $\mu_{C_{(2,2)}} \approx 2$. The parameters were chosen as above, but: $n_{\mathrm{sim}} = 10^5$, $n_1 = 0$, $n_2 = 5 \times 10^{10}/\mathrm{m}^3$, which results in only evaluating $\beta_{2,2}$, as no particles of size v_1 are initialized. The coefficient of variation is estimated to $\tilde{\theta}_{\hat{\beta}_{(2,2)}} = 69.88\%$, where the confidence limits are $70.55\% < \theta_{\hat{\beta}_{(2,2)}} < 70.97\%$. It follows, that the results of Section 5, especially Eq. (22), can be safely used for simulations with $\mu_{C_{(i,j)}} > 4$. However, if $\mu_{C_{(2,2)}}$ further decreases, the coefficient of variation will become $\theta_{\hat{\beta}_{(2,2)}} > 100\%$. As no negative aggregation-rate kernels can be calculated, this truncates the probability and frequency distribution on the left, which can already be observed in Fig. 6.

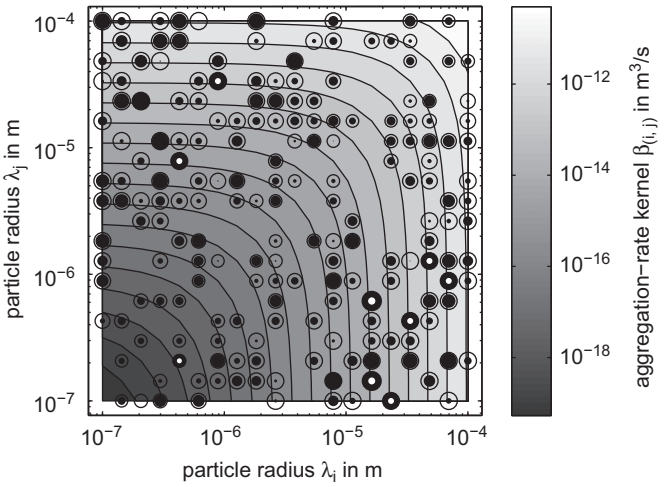

Fig. 7. Aggregation-rate kernels for a broad spectrum of particle sizes, detailed description in text.

6.3. Simulation results for a broad spectrum of particle sizes

In this section simulations are presented to cover the aggregation-rate kernels of particle sizes between 0.1 and 100 μm. The spectrum of particle sizes was divided into 20 intervals, which are equally sized on a logarithmic axis and the results are shown in Fig. 7.

In each simulation only two distinct particle sizes are initialized to evaluate the corresponding aggregation-rate kernel directly. Aggregation-rate kernels of equally sized aggregation partners can be calculated from the executed simulations by a weighted empirical mean using the estimation of the coefficient of variation in Eq. (22). These aggregation-rate kernels are not considered in this contribution, as the results are far more accurate and could not be visualized in Fig. 7. The simulation parameters for 190 simulations are $\gamma = 5\ \mathrm{m\ s^{-1}}$, $N = 64 \times 10^3$, $T_{\mathrm{sim}} = 0.2$ s and $k_\lambda = 1/30$. The particle-mass fraction is adjusted to $\varphi = 5\%$ by setting $n_1 = n_2 = \varphi/(v_1 + v_2)$.

The background in Fig. 7 together with the legend shows the spectrum of the covered aggregation-rate kernels. The estimated coefficients of variation (circles) and the calculated relative errors (filled circles) are plotted in a way to visualize the most important information.

The relative error is proportional to the area of the filled circle: $a_\delta = K\delta_{\hat{\beta}}/\max_{(i,j)}(\tilde{\theta}_{\hat{\beta}_{(i,j)}})$ and the coefficient of variation is proportional to the area of the unfilled circles: $a_{\tilde{\theta}} = 2K\tilde{\theta}_{\hat{\beta}_{(i,j)}}/\max_{(i,j)}(\tilde{\theta}_{\hat{\beta}_{(i,j)}})$. This means, the maximum sized circle corresponds to the maximum of all coefficients of variation, which is 4.6% and a filled circle of the same maximum size corresponds to a relative error of 9.2%. From the normal distribution of the simulation results it is known that 95.4% of the achieved relative errors are smaller than twice the coefficient of variation, from which follows that approximately nine filled circles should be larger than the unfilled circles. Where the absolute value of the relative error is larger than twice the estimated coefficient of variation, the data points are marked with a small white filled circle. As the aggregation-rate kernels are symmetric ($\beta_{(i,j)}$ equals $\beta_{(j,i)}$) it was decided to put positive relative errors in the upper left corner and negative relative errors in the lower right corner.

The reason for choosing this rather complex visualization is the amount of information it contains. A higher number of intervals were investigated as to whether they revealed any kind of significant structure or deviation that would easily catch the eye. However, this was not the case. Nine relative errors are larger than twice the estimated coefficient of variation, which is in good agreement. As the amount of data points or the total area of the filled circles does not accumulate at some point in the figure, no deviation is observed. The following deviations could be possible. For a general deviation, more data points would be located in the upper left or lower right corner. Deviations involving simulation of particle pairs of very different sizes would cause the number of data points to increase or decrease from the symmetry axis to the outer corners. Alternatively, deviations involving simulations of large particles would cause the homogeneity to decrease in the direction of the upper right corner.

No significant structure can be observed in Fig. 7 and, hence, the discrete element model and the derivations in this contribution are validated even for a very broad spectrum of particle sizes.

6.4. Fitting the parameter k_λ

To fit an appropriate value for the parameter k_λ, which limits the displacement of particles in the system per time step, sets of

10^5 simulations were evaluated. Different values k_λ were set while using the same sequence of seeds for the random-number generator. Apart from n_{sim} the same set of parameters applies as in the beginning of Section 6.2. Fig. 8 shows the relative errors for the different aggregation partners and the confidence limits in light lines. For $k_\lambda = 0.1$, $\hat{\beta}_{2,2}$ and $\hat{\beta}_{1,2}$ show a significant deviation from the confidence interval. The relative errors are -0.0659% and -0.0965%, respectively, where the confidence limits are $\pm 0.0576\%$ and $\pm 0.0627\%$, respectively. Furthermore, the slopes of the relative errors are identical. With respect to Eq. (10), the derivation of the time step limit is independent from particle sizes, which explains this observation. However, this will not necessarily apply when different aggregation mechanisms are investigated. The parameter k_λ is set to $k_\lambda = 1/30$ for the coupling with the population balance model.

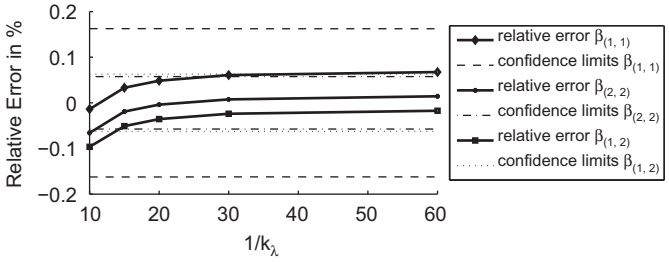

Fig. 8. Relative errors of aggregation-rate kernels in dependence of parameter k_λ.

7. Multiscale simulations

For the presented case study, the initial condition is $\tilde{n}(v,0) = 0$. The growth constant is set to $k_g = 1.2 \times 10^{-6}$ m s^{-1}. The nucleation rate is $\sigma_{nuc}(v = 1 \times 10^{-14}\ \text{m}) = 1 \times 10^{10}$ s^{-1}. The discretization used initially 10 intervals per decimal power of the particle volume and the integration time steps were set to 50 ms. Each time step, a single discrete element simulation is evaluated using the current particle densities $\underline{n}$, the shear rate $\gamma = 3.5$ s^{-1}, $N = 5 \times 10^4$ particles and a total simulation time of $T_{sim} = 100$ m s. This multiscale model was compared to the same model, but using the analytical aggregation-rate kernel instead of discrete element simulations (Fig. 1). The evolution of the corresponding particle-size distribution is shown in Fig. 9.

The particle-size distribution is in excellent agreement for at least 99% of the total particle volume, which is shown in Fig. 9 by a large star placed in the position of 99% of the total particle volume, if integrated from the left. The deviations are caused by the discrete nature of the microscale level. If no collisions are counted, the aggregation-rate kernel is zero and if all aggregation-rate kernels $\beta(v_i, v_j - v_i)$ are zero, the birth rate of particles of size v_j is zero. This happens if the coefficient of variation is much larger than 100%. In extreme cases, there is a very high probability that no collisions are counted and it is $\hat{\beta}_{(i,j)} = 0$, while counting one collision is very unlikely but this would yield $\hat{\beta}_{(i,j)} \gg \beta(v_i, v_j)$. Hence, increasing the accuracy of the discrete element simulations improves the result, which is shown in Fig. 10. The parameters are changed to $N = 2 \times 10^5$ and $T_{sim} = 200$ m s, which decreases the coefficient of variation to 35% of the preceding simulations (Eq. (22)). The large stars

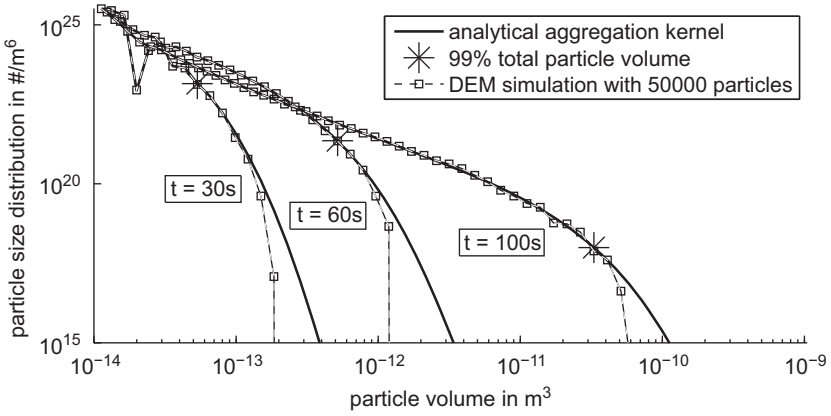

Fig. 9. Evolution of particle-size distributions for an analytical kernel (bold) and an aggregation-rate kernel obtained *via* discrete element simulation (dashed).

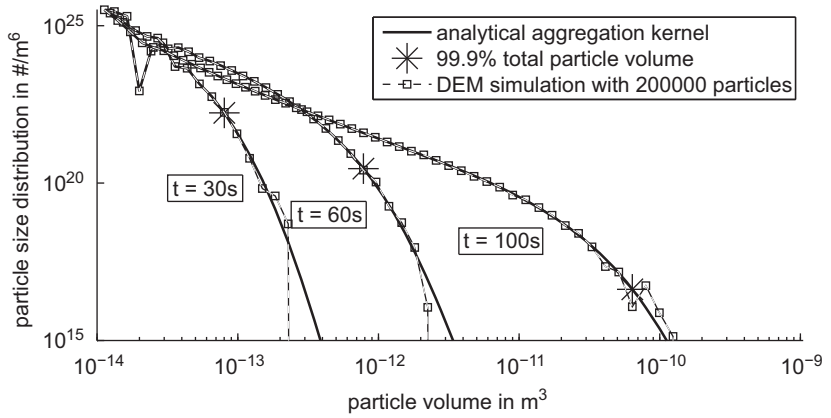

Fig. 10. Evolution of particle-size distributions for an analytical kernel (bold) and an aggregation-rate kernel obtained *via* discrete element simulation (dashed).

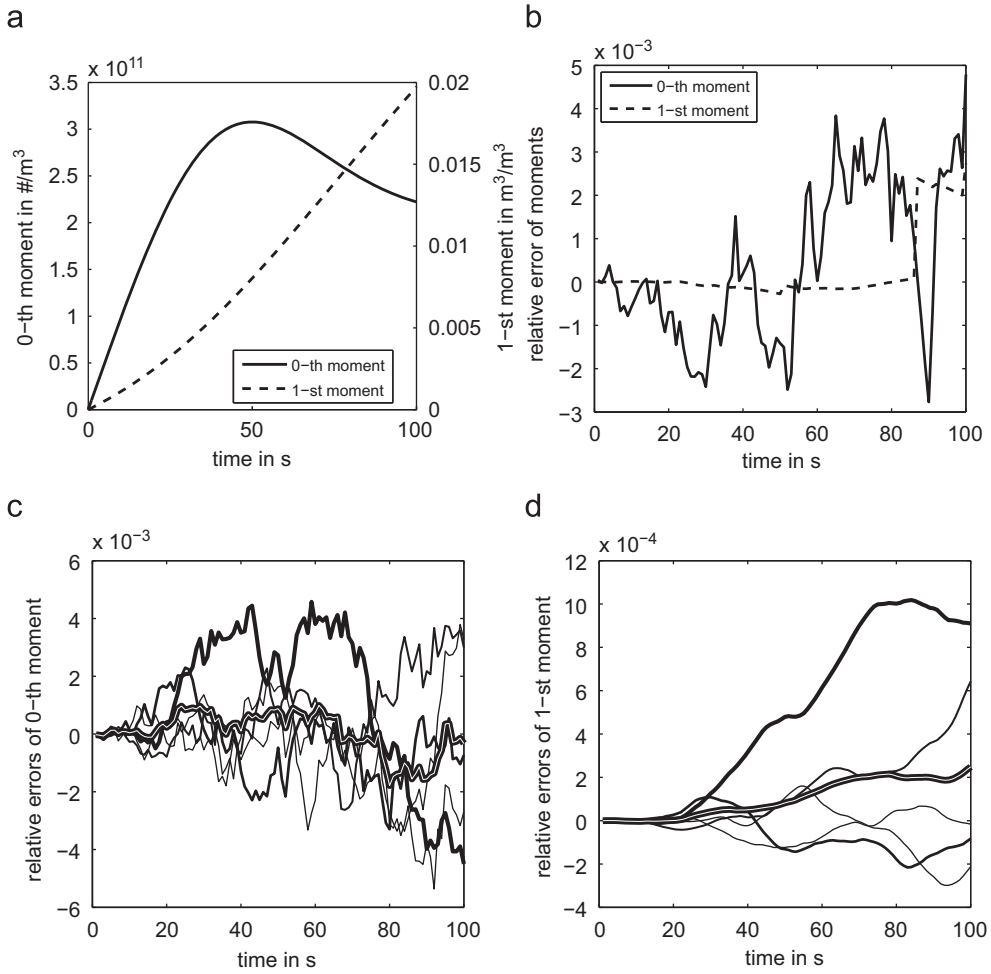

Fig. 11. Time evolution of moments and relative error of moments. (a) 0th and 1st moment, (b) relative errors 0th and 1st moment of a simulation with $\Delta T = 0.5$ s and $n_{\mathrm{sim}} = 2 \times 10^5$, (c) relative errors of 0th moment of simulations with $\Delta T = 0.05$ s and $n_{\mathrm{sim}} = 5 \times 10^4$, relative error of mean particle-size distribution is drawn striped, (d) relative errors of 1st moment of simulations with $\Delta T = 0.05$ s and $n_{\mathrm{sim}} = 5 \times 10^4$, relative error of mean particle-size distribution is drawn striped.

represent now 99.9% of the total particle volume. For $t = 100$ s the particle density is even overestimated, which shows that the random deviations affect the particle density values in both directions. The simulation for Fig. 9 took about 2 h on a desktop computer, the simulation for Fig. 10 took 17 h.

The plot in Fig. 11(a) shows the evolution of the 0th moment (total particle number) and 1st moment (total particle volume) of the particle-size distribution over time. The Fig. 11(c) and (d) shows the relative errors of these moments for five stochastically independent multiscale simulations with the parameter set initially presented in this section. Additionally, the mean of the five particle-size distributions is calculated for each time and the resulting relative error is added to these plots using a striped line.

For the 0th moment, the relative errors spread equally around zero, as the total particle number is directly affected by aggregation. The amplitude of the deviation seems to increase equally in both directions, where the relative error is smaller than 0.5%.

The relative errors of the 1st moment deviate slowly from zero and seem to increase significantly over time. Nucleation changes particle number and total particle volume, but the multiscale and reference model are equally influenced by this mechanism. Aggregation does not effect the total particle volume directly, but it is connected to the total particle volume *via* growth. From the growth term (Eq. (2)) it follows that overestimating the total particle number has less effect on the total particle volume than underestimating the total particle number. Two small sized particles accumulate more solid matter than one larger particle of the same total particle volume. This effect is connected to $G \sim v^{2/3}$, an exponent smaller than one yields the observed results, while an exponent larger than one would cause deviations in the direction of negative relative errors. The deviation of the 1st moment is nearly an order of magnitude smaller than the deviations of the 0th moment.

The plot in Fig. 11(b) shows the evolution of the relative errors of the 0th and 1st moment of a simulation with integration time steps of the population balance solver set to 500 m s and $N = 2 \times 10^5$. Steps in the relative error of the 1st moment can be observed. These steps occur if aggregation-rate kernels are highly overestimated so that the death rate of aggregation multiplied by the step size of the population balance solver is larger than the particle density in the corresponding discretized bin. This problem can either be solved by increasing the accuracy of the discrete element model or by decreasing the step size of the population balance solver. The latter one can be seen in Fig. 11(c) and (d). The coefficient of variation of the underlying discrete element simulations is two times larger, but the simulation time steps of the population balance solver are ten times smaller.

8. Conclusions

The analytical aggregation-rate kernel for shear-induced aggregation was accurately reconstructed using a discrete element model,

which was validated in detail. Just having a microscale model, which reconstructs an already available analytic expressions is, of course, of minor importance. However, the details of the presented model contain references to pitfalls, which must be avoided in more complicated cases, where no analytic kernel is available for validation. Furthermore, the stochastic analysis of the model leads to an equation, which may be of major importance for further studies. Eq. (22) connects the parameters on the level of the population balance model to the accuracy of the discrete element simulation. For further research, this permits the investigation of more complex multiscale approaches, which preserve a certain degree of accuracy under consideration of the necessary total particle number and simulation time and, hence, the computational effort of the microscale simulation.

By understanding the nature of the underlying discrete element simulation, these computational expensive evaluations are not necessary any more to study the behavior of the multiscale model. Instead of running the discrete element simulations an analytic expression can be used, which is modified by normally distributed random deviations using a standard deviation from Eq. (22) and correct aggregation-rate kernels smaller than zero by setting them to zero, if necessary. If the estimated coefficient of variation is very large, a binomially distributed number of counted collisions should be assumed to model the probability distribution of the statistically evaluated aggregation-rate kernel $\hat{\beta}$. In summary, the partial integro-differential equation, the population balance, becomes more complex using this multiscale approach and results in a *stochastic* partial integro-differential equation.

An excellent agreement can be achieved for a high fraction of the total particle volume. Few studies have been performed to explore the variety of possible multiscale models. As the heterogeneous multiscale modeling is a data-driven approach, the behavior of the multiscale simulation results *may* depend on the solution method for the population balance model, for which a high variety exists. Furthermore, the drift of the 1st moment is a biased deviation dependent on the exponent of the particle volume in the term of the growth rate. The order of magnitude of this error is small, but in realistic situations this error may become a serious problem.

Instead of using the aggregation-rate kernel, the birth and death rates for aggregation should be directly calculated by the discrete element model because the introduction of aggregation rates and aggregation-rate kernels is not necessary. However, this does not mean to ignore the fruitful approach of evaluating particle collisions and collision efficiency separately (Mumtaz et al., 1997; Gantt and Gatzke, 2006).

Nomenclature

Greek letters

$\tilde{\beta}$,$\hat{\beta}$	analytical and estimated aggregation-rate kernel, m^3/s
γ	shear rate, 1/s
λ,λ_k	particle radius and representative particle radius of size interval k, m
λ_{max}	maximal particle radius for a DEM simulation, m
$\mu_{(\cdot)}$	expectation value of a random variable
$\sigma_{(\cdot)}$	standard deviation of a random variable
σ_{nuc}	nucleation rate, $1/m^6$ /s
$\theta_{(\cdot)}$	coefficient of variation of a random variable

Symbols

$C_{(i,j)}$	counted collisions for particles of size intervals i and j, –
G	growth rate, m/s
k_λ	parameter to limit DEM simulation time steps, –
N, N_k	total number of particles or number of particles for a spezific size class k of a DEM simulation, –
n_{int}	number of particle size intervals, –
$\tilde{n}$	particle size distribution, $1/m^6$
p_k	a specific particle, –
P_{coll}	probability of observing a collision between particles of size intervals i and j, –
P_i	probability of a particle to have the size interval i, m^3
P_{init}	probability of detecting collisions just after initialization, –
r	aggregation rate, $1/m^9$ /s
T_{sim}	simulated time for a DE model, s
v, v_k	particle volume and representative particle volume of size interval k, m^3
V_{obsv}	volume observed for collision detection in DEM, m^3
V_{sim}	total volume for DEM simulation, m^3
x_{width}, y_{width}, z_{width}	dimensions of the simulated box for the DE-model, m

Acknowledgments

We thank Dr. Anthony M. Reilly for proof reading a draft of this paper.

References

Beyer, O., Hackel, H., Pieper, V., Tiedge, J., 1995. Wahrscheinlichkeitsrechnung und Mathematische Statistik. B.G. Teubner Verlagsgesellschaft, Leipzig.
Cundall, P.A., Strack, O.D.L., 1979. Discrete numerical-model for granular assemblies. Géotechnique 29, 47–65.
Gantt, J.A., Gatzke, E.P., 2006. A stochastic technique for multidimensional granulation modeling. AIChE Journal 52, 3067–3077.
Heine, M.C., Pratsinis, S.E., 2007. Brownian coagulation at high concentration. Langmuir 23, 9882–9890.
Hounslow, M.J., Mumtaz, H.S., Collier, A.P., Barrick, J.P., Bramley, A.S., 2001. A micro-mechanical model for the rate of aggregation during precipitation from solution. Chemical Engineering Science 56, 2543–2552.
Kevrekidis, I.G., Gear, C.W., Hummer, G., 2004. Equation-free: The computer-aided analysis of complex multiscale systems. AIChE Journal 50, 1346–1355.
Kumar, S., Ramkrishna, D., 1997. On the solution of population balance equations by discretization – III. Nucleation, growth and aggregation of particles. Chemical Engineering Science 52, 4659–4679.
Mumtaz, H.S., Hounslow, M.J., Seaton, N.A., Paterson, W.R., 1997. Orthokinetic aggregation during precipitation: a computational model for calcium oxalate monohydrate. Chemical Engineering Research and Design 75, 152–160.
Pöschel, T., Schwager, T., 2005. Computational Granular Dynamics: Models and Algorithms. Springer, Berlin.
Ramkrishna, D., 2000. Population Balances—Theory and Applications to Particulate Systems in Engineering. Academic Press, San Diego.
Reinhold, A., Briesen, H., 2009. Discrete element modeling for multiscale simulation of aggregation processes. In: Tenth International Symposium on Process Systems Engineering – PSE2009.
Smoluchowski, M., 1917. Versuch einer mathematischen Theorie der Koagulationskinetik kolloider Lösungen. Zeitschrift für Physikalische Chemie 92, 129–168.
Trzeciak, T.M., Podgórski, A., Marijnissen, J.C.M., 2004. Langevin dynamics simulation of aerosol coagulation in highly concentrated systems. Inzynieria Chemiczna i Procesowa 25, 1741–1746.
Trzeciak, T.M., Podgórski, A., Marijnissen, J.C.M., 2006. Stochastic calculation of collision kernels: Brownian coagulation in concentrated systems. In: World Congress on Particle Technology – WCPT5.
Weinan, E., Enquist, B., Li, X.T., Ren, W.Q., Vanden-Eijnden, E., 2007. Heterogeneous multiscale methods: a review. Communications in Computational Physics 2, 367–450.